Journal of
Composites Science

MDPI

Article

Effect of Copper Doping in Borate Bioactive Glass on Bacterial Colonization Prevention—An Insight Study on Protein/Carbohydrate Leakage for Biomedical Applications

Bharath Sankaralingam [1], Gobi Saravanan Kaliaraj [1,*], Isha Rameshbabu [2], Padmapriya Rajendran [2] and Kamalan Kirubaharan Amirtharaj Mosas [3,*]

[1] Centre for Nanoscience and Nanotechnology, Sathyabama Institute of Science and Technology, Chennai 600119, India; bharathsankaralingam123@gmail.com
[2] PG Department of Biochemistry, Auxilium College (Autonomous), Gandhinagar, Katpadi, Vellore 632006, India; isharamesh1616@gmail.com (I.R.); padmapriya2965@gmail.com (P.R.)
[3] Coating Department, Fun Glass—Centre for Functional and Surface Functionalized Glass, Alexander Dubcek University of Trencin, 91150 Trencin, Slovakia
* Correspondence: gobisaravanan@sathyabama.ac.in (G.S.K.); kamalan.mosas@tnuni.sk (K.K.A.M.)

Abstract: Researchers have extensively studied borate bioactive glass (BBG) for bone regeneration and wound healing applications. In the current study, 13-93B3 (54.6% B_2O_3, 22.1% CaO, 7.9% K_2O, 7.7% MgO, 6.0% Na_2O, and 1.7% P_2O_5) was synthesized using a sol–gel technique and doped with different molar concentrations of Cu (0.01, 0.05, and 0.25 M) into BBG for possible biomedical applications. Then, the antibacterial activity was tested against *E. coli* and *S. aureus*. The maximum zone of inhibition against *S. aureus* was achieved at 100 µg/mL of 0.25 M Cu-doped BBG. At 50 µg/mL of 0.25 molar copper concentration, *E. coli* showed a significant reduction in colony-forming units. Hydroxyl radical production, influenced by the BBG powder, was most effective against *S. aureus*, followed by *E. coli*. Protein leakage studies demonstrated significant leakage after treatment with BBG powder, demonstrating a strong effect on bacterial strains. This shows a change in protein synthesis, which is essential for central metabolism and gene transcription, affecting proteins in the periplasm and inner and outer membranes. Furthermore, carbohydrate leakage studies showed that BBG is effective against all three categories of cellular carbohydrate, namely membrane-bound, transmembrane, and intracellular carbs. This study focuses on the diverse antibacterial processes of Cu-doped BBG, which has emerged as a promising contender for biological applications that require strong antibacterial characteristics.

Keywords: borosilicate glass; antimicrobial activity; protein leakage; carbohydrate leakage; biomedical applications

Citation: Sankaralingam, B.; Kaliaraj, G.S.; Rameshbabu, I.; Rajendran, P.; Amirtharaj Mosas, K.K. Effect of Copper Doping in Borate Bioactive Glass on Bacterial Colonization Prevention—An Insight Study on Protein/Carbohydrate Leakage for Biomedical Applications. *J. Compos. Sci.* **2024**, *8*, 245. https://doi.org/10.3390/jcs8070245

Academic Editor: Francesco Tornabene

Received: 15 May 2024
Revised: 13 June 2024
Accepted: 24 June 2024
Published: 28 June 2024

1. Introduction

Microbial corrosion and biofilm formation are serious challenges in biomaterials, destroying the materials' overall performance and integrity. An enormous amount of biomaterial is employed in the healthcare sector to promote patient health, including dental prosthesis, heart valves, stunts, meshes, and so on. They are mostly composed of metals, polymers, ceramics, or a combination of all three [1]. Humans have a symbiotic relationship with many microbial organisms, including some potential pathogens [2]. All implanted materials will come into contact with biological tissues and bodily fluids. Bacteria or any microbial species can colonize on the surface of the biomaterial if there are any suitable micro-environments such as temperature and moisture. Biomaterials frequently provide a surface for initial adhesion, which is critical for biofilm formation [3].

Biofilm is a substance formed by microbial cells after microbes adhere to the surface of biomaterials. Biofilm is an extracellular polymeric substance (EPS) that contains mainly

polysaccharides, proteins, DNA, RNA, and lipids. These molecules provide extra support and protection against environmental stresses after the initial adhesion. But the initial adhesion is only determined by the physiochemical properties of the surface and microbes [4]. Sometimes these chemicals may compromise the integrity of biomaterials by inhibiting their bioactivity and interfering with their intended function [5]. Many microbes can produce acids and enzymes as metabolic byproducts. Acids and enzymes (proteases and lipases) break down biomaterials and break down their organic components. Biomaterials may also release the ions needed for cellular growth, healing, or function. However, microbial activity can interfere with ion exchange, altering ion release and lowering biomaterial functionality [4,6]. The accumulation of these organic compounds on the biomaterial (biofouling) will hinder the interaction between biomaterials and the surrounding cells. As a result, microbial colonization will affect the surface, topography, and chemistry of active biomaterials. This change would influence cell adhesion, proliferation, and differentiation on the material's surfaces [7].

The primary objective of any synthesized biomaterials, as well as their intended application, is to inhibit cell multiplication and destroy or stop the proliferation of microbial cells. BBGs are the most commonly used in biomedical applications. BBG derivatives, in particular, are employed as temporary bioactive surfaces in a wide range of applications, including bone tissue engineering, which includes wound healing, targeted drug delivery, and other regenerative medicine.

The primary and essential characteristics of any synthesized biomaterials are their antibacterial capabilities and improved biomaterial surface qualities for long-term life. Several strategies are designed to work together with all attributes to improve materials' physiochemical and biological properties. The addition of therapeutic ions such as Cu into bioactive glass composition improves its intrinsic capabilities by disturbing the plasma membrane, modulating oxidative processes, causing DNA damage, and so on [8,9].

BBG plays an important role in bone regeneration and is promising for chronic wound treatments. It is produced by replacing silica ions with boron in the glass network. Borate is the trace element available in the body and plays a pivotal role in bone regeneration. Boron elements promote calcium integration into cartilage, bones, and joints. Importantly, the presence of boron in the body reduces the symptoms of arthritis, osteoporosis, and coronary heart diseases [10].

To the best of our knowledge, there have been enough studies conducted to determine the bactericidal activity of bioactive glass. However, there are no available studies in the literature investigating protein/carbohydrate leakage and hydroxyl radical production by bacterial strains against BBG. Therefore, the current study focuses on generating 13-93B3-based BBG (mol.%: 54.6% B_2O_3, 22.1% CaO, 7.9% K_2O, 7.7% MgO, 6.0% Na_2O, and 1.7% P_2O_5) with varying Cu molar concentrations by sol–gel synthesis for biologically rich and antimicrobial active surfaces in biomedical applications. The structure and morphology of prepared BBGs were also examined.

2. Materials and Methods

2.1. Borate Bioactive Glass Synthesis

The sol–gel method was utilized to synthesis BBG powders, designated 13-93B3, containing 54.6% B_2O_3, 22.1% CaO, 7.9% K_2O, 7.7% MgO, 6.0% Na_2O, and 1.7% P_2O_5. The precursors employed in the process of production included triethyl phosphate (TEP), calcium nitrate tetrahydrate ($Ca(NO_3)_2{\cdot}4H_2O$), potassium nitrate (KNO_3), magnesium nitrate hexahydrate ($Mg(NO_3)_2{\cdot}6H_2O$), sodium nitrate ($NaNO_3$), copper nitrate ($CuNO_3$), and tributyl borate (TBB).

First, 12 mL of TBB was added to a 40 °C solution containing 13 mL of ethanol, an equal amount of water, and 0.1 mL of HNO_3. The mixture was agitated for approximately 60 min at 600 rpm. The doped (three different concentrations, Table 1) and undoped samples were then mixed with a magnetic stirrer. For undoped sample BBG synthesis, 0.54 mL of TEP, 0.72 g of sodium nitrate ($NaNO_3$), 5.90 g of calcium nitrate ($Ca(NO_3)_2{\cdot}4H_2O$), 2.82 g

of magnesium nitrate ($Mg(NO_3)_2 \cdot 6H_2O$), and 1.31 g of potassium nitrate (KNO_3) were added in only when the prior step's solution was clear. For Cu doping, three different concentrations of $Cu(NO_3)_2 \cdot 3H_2O$ (0.05, 0.5, and 0.25 M) were added to the sol and stirred for 5 h. The solution was allowed to age overnight after stirring. The sol was washed with distilled water, centrifuged, and dried at 600 °C for 5 h (Cu-doped samples) [10].

Table 1. Different molar concentrations of copper-doped BBG's.

Chemicals	$CuNO_3$ (Molar Concentration)		
	0.25	**0.05**	**0.01**
TEP	0.54 mL	0.54 mL	0.54 mL
Sodium nitrate ($NaNO_3$)	0.72 g	0.72 g	0.72 g
Calcium nitrate ($Ca(NO_3)_2 \cdot 4H_2O$)	2.95 g	5.31 g	5.31 g
Magnesium nitrate ($Mg(NO_3)_2 \cdot 6H_2O$)	3.02 g	0.64 g	0.64 g
Potassium nitrate (KNO_3)	1.31 g	1.31 g	1.31 g
Copper nitrate ($CuNO_3$)	3.20 g	0.60 g	0.12 g

2.2. Characterization of BBG Powder

To determine the crystalline nature, the produced BBG powder was analyzed using X-ray diffraction (XRD, Bruker, Billerica, MA, USA). The surface morphology and elemental composition of BBG were evaluated using a field emission scanning electron microscope (FESEM, SUPRA, Carl Zeiss, Jena, Germany) equipped with energy-dispersive X-ray spectroscopy (EDS). Raman spectroscopy was performed with a Renishaw Invia Reflex confocal Raman microscope. X-ray photoelectron spectroscopy (Thermoscientific K-alpha, Waltham, MA, USA) was employed to study the chemical constituents.

2.3. Hydroxyl Radical Generation

DMSO traps damaging hydroxyl radicals (OH•) in biological systems. It is oxidized by OH radicals to produce a stable, easily detectable molecule known as methanesulfinic acid. This method enables the straightforward and inexpensive assessment of cumulative OH radical production in biological samples treated with DMSO [11,12]. BBG samples with various $CuNO_3$ molar concentrations were prepared, followed by dispersing a known weight in each 1 mg/mL amount of bacterial solution. A control group comprising simply the bacterial solution and no glass samples should also be prepared. To capture hydroxyl radicals, add 28.2 mL DMSO to all samples and controls. Following the addition of DMSO, rotate the samples and control at 37 °C for the desired time interval. Using a syringe filter (2.5 mm pore size), extract 2.5 mL aliquots from each at regular hourly intervals. In each aliquot, add 2.5 mL of pH 4 buffer solution and 0.5 mL of DPNH (2,4-dinitrophenylhydrazine) solution. Then, heat the solutions to 40 °C for the specified time. Finally, cool the solutions before measuring their absorbance at 360 nm with a spectrophotometer [13].

2.4. Minimum Inhibitory Concentration

Initially, a pure microbial culture was prepared by streaking on agar plates. This was followed by an overnight incubation period to promote colony growth. The next stage was to initiate a liquid culture and allow it to go through the mid-logarithmic development phase. The bacterial inoculum was painstakingly prepared and condensed to the appropriate level. The test substance was then applied in various concentrations to sterile discs/created wells in agar plates. The test material was incubated at 37 °C, and after the specified period, the diameters of the inhibition zones surrounding it were precisely measured to determine the antibacterial efficacy of the BBG powder.

2.5. Colony-Forming Unit

To make a broth culture, use the same concentrations of BBG (*E. coli* and *S. aureus* bacteria) per milliliter of broth. The broth was thoroughly mixed with test samples and evenly dispersed after three to four hours of bacterial growth. Using a sterile spreader, 30 µL of the incubated material was pipetted onto agar plates and then evenly distributed. Then, the agar plates were incubated for a suitable period of time and temperature to support the growth of the specific microbiological sample. Following incubation, the colony-forming units (CFUs) on the agar plates were counted, and the total CFU count for each plate was recorded. Each test was performed in triplicate.

2.6. Protein Discharge Assay

We examined the protein efflux capabilities of borosilicate glasses doped with various Cu concentrations for possible biomedical applications. $CuNO_3$ solutions at concentrations of 1 mg/mL (0.01, 0.05, and 0.25 M) were added to a 24 h culture of *E. coli* and *S. aureus* bacteria. The centrifugation process was used to separate the proteins produced by the bacterial cells following a 4–5 h incubation period at 37 °C. The extracted proteins were subjected to the Bradford assay, with absorbance measured at 595 nm after 10 min of incubation in the dark.

2.7. Carbohydrate Discharge Assay

The carbohydrate discharge assay was carried out against *E. coli* and *S. aureus* bacteria using Cu-doped and undoped BBG. Carbohydrate leakage was used to assess the discharge capacity of carbohydrates, glycolipids, and glycoproteins in bacterial strains in the presence of Cu-doped and undoped BBG powder. Cu-doped and undoped BBG powders (1 mg/mL) were added to a 24 h culture of *E. coli* and *S. aureus* and cultured for 4–5 h. Following incubation, the samples were treated with anthrone reagent and put in a water bath at 50 °C for 10 min. The liberated carbohydrates from the bacterial cell walls were then separated by centrifugation. The anthrone reagent was added, and the absorbance measurements were taken at 620 nm. The concentration of carbohydrates was then determined by comparing the absorbance readings to a glucose standard curve.

2.8. Live/Dead Cell Analysis

Acridine orange is a fluorescent cationic dye that selectively stains nucleic acids and can cross cell membranes, staining both living and dead cells. Acridine orange is applied to the microbiological samples prior to fluorescence microscopy. This permits the dye to penetrate the cells and attach to nucleic acids, which subsequently fluoresce green when exposed to the right amount of light. Undamaged nucleic acids are identified by a continuous green fluorescence that can be seen throughout living cells. On the other hand, dead cells may exhibit unique fluorescence patterns, such as feeble or punctuated fluorescence, indicating weaker nucleic acids. This technique allows for the detection and assessment of viable microbial populations inside a sample by contrasting the fluorescence patterns of living and dead cells [14,15]. Acridine orange (AO) was mixed in 100 mL of acetate buffer to create a solution that could be used to image both dead and living microbial cells using fluorescence. Before staining, microbial broth cultures (*E. coli* and *S. aureus*) cultured for 24 h were used. One microgram of each sample was mixed with 1 mL of broth and incubated for four to five hours. Following the incubation period, the samples were dyed using the prepared dye solution for 10 min. The stained samples were then gently rinsed with phosphate-buffered saline (PBS) and photographed with a Nikon epifluorescence microscope (Japan).

3. Results and Discussion

3.1. Characterization of BBG Powders Using XRD, Raman Spectroscopy, and FESEM

13-93B3-based BBG was synthesized using the sol–gel method. As mentioned in the previous study by Bento et al., 2021, the sol–gel method might end up producing a

substance of an amorphous nature [16]. The sequential addition of precursors, including sodium nitrate, calcium nitrate tetrahydrate, magnesium nitrate hexahydrate, potassium nitrate, and triethyl phosphate, supports the gel formation that occurred through hydrolysis and condensation reactions, followed by evaporation-induced solidification producing the powdered bioactive glass discussed by Deliormanli [10]. Low sodium concentrations in the process may change the activity of glass and gel formation during synthesis, which also requires a high pH [15]. The structural and morphological properties of the generated BBG powders were investigated using XRD, FESEM, and Raman spectroscopy.

Figure 1 shows the surface morphology of undoped (Figure 1a) and Cu-doped BBG (Figure 1b–d). The particle size of BBG was around 100–200 nm in its undoped form, and the particle size was slightly reduced with copper concentrations in Figure 1b,c. Further, a higher Cu dopant concentration resulted in substantially smaller particle sizes (Figure 1d). The reduction in the particle size of BBG and Cu-doped BBG is due to the dopant copper ions (Cu^{2+}), which substitute host lattices (B_2O_3, MgO, CaO, and Na) and distort their lattice structures, resulting in a reduction in particle size variation with different concentrations of Cu [17].

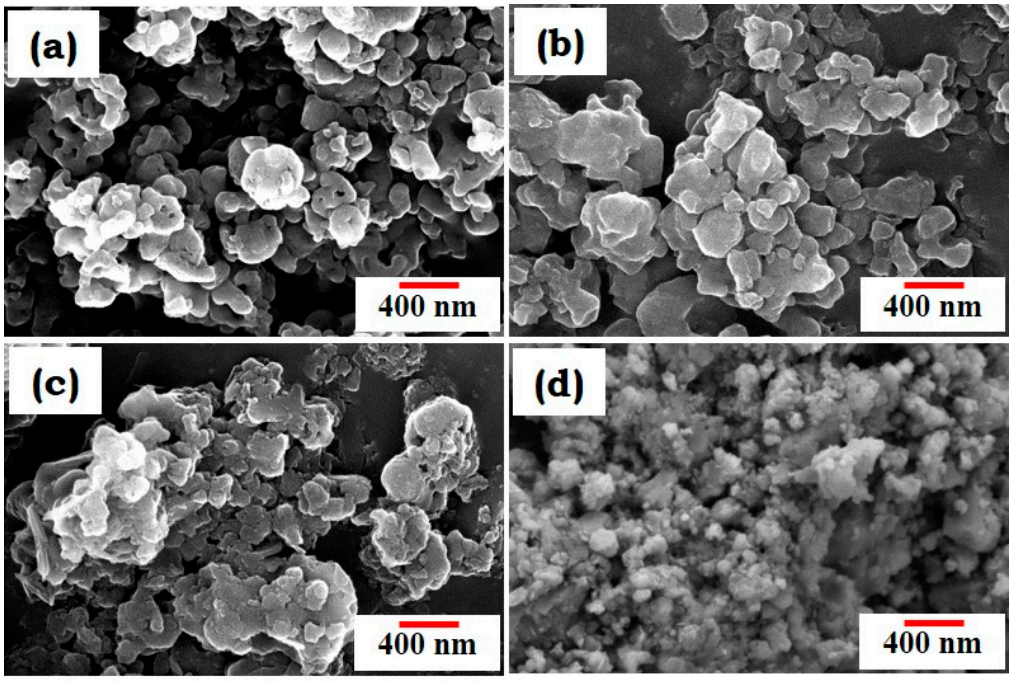

Figure 1. Surface morphology of (**a**) BBG, (**b**) 0.01 M Cu-doped BBG (**c**), 0.05 M Cu-doped BBG, and (**d**) 0.25 M Cu-doped BBG.

Raman spectra of BBG doped with different concentrations of Cu show distinct peaks corresponding to specific vibrational modes within the glass network (Figure 2). The prominent peaks at 1053 cm^{-1} for undoped, 0.01, 0.05, 0.25, and Cu doping suggest the presence of B-O stretching vibrations in borate triangles or tetrahedra, potentially driven by the creation of Cu-O bonds or alterations to the borate network produced by copper [18]. The strong peak around 1053 cm^{-1} remains consistent throughout doping levels, including 0.25% Cu, indicating the presence of a stable structural motif, probably a Cu-B-O complex. The presence of a peak at 1053 cm^{-1} in all BBG samples suggests an unchanged borate network structure. These findings provide significant insight into the structural changes caused by copper doping in the BG network, allowing for a better understanding of the composition–structure–property relationship [18–20].

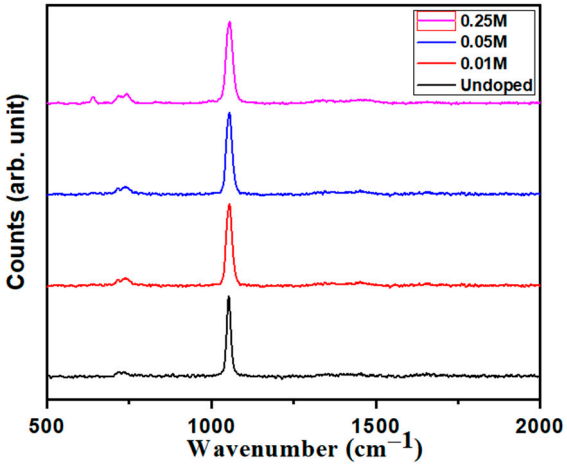

Figure 2. Raman spectra of Cu-doped and undoped borate bioactive glass for functional group analysis.

X-ray diffraction (XRD) analysis (Figure 3) revealed a shift in the peak positions with increasing Cu doping levels, indicating a change in the material's structure [21]. While Raman spectroscopy confirmed the expected bonding environment in pristine BBG, XRD identified the presence of crystalline Cu-O-B phases in Cu-doped BBG, as evidenced by diffraction peaks matching the reference pattern for this structure (JCPDS card no. 48-1548) at 35° [22]. The presence of sodium nitrate (JCPDS number 36-1474) with a rhombohedral lattice phase corresponding to the (104) plane at 29° was also detected in the BBG samples [10]. This sodium nitrate likely aids in the formation of sodium borate (JCPDS card no. 37-0115), another rhombohedral phase with a peak at 33.9° corresponding to the (012) plane [10]. Interestingly, glasses with lower Cu dopant concentrations exhibited fewer sharp peaks, indicative of an amorphous structure that is a desirable characteristic for bone regeneration applications. Conversely, higher dopant levels led to the emergence of distinct diffraction peaks, suggesting the formation of crystalline phases [23,24]. This observation suggests that Cu ions become incorporated into the borate glass matrix at the molecular level, inducing a transition from a disordered (amorphous) to a more ordered (crystalline) structure. These findings provide valuable insights into the spatial and physical properties of the Cu-doped BBG material, offering valuable information on its structural evolution and potential applications [25].

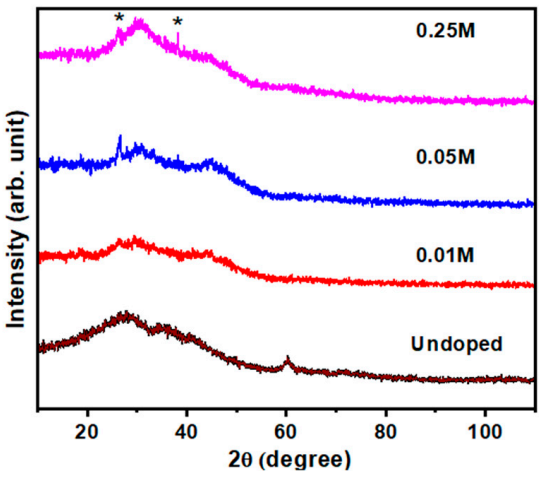

Figure 3. XRD structural modification and treatment elucidation analysis with different dopings of copper. * indicates peak positions.

3.2. X-ray Photoelectron Spectroscopy Analysis

The X-ray photoelectron spectroscopy (XPS) technique was employed to determine the chemical state of copper (Cu) in the doped borate bioactive glass (Figure 4). From the survey spectrum, all the elements (Na, K, Cu, B, Mg, Ca, and P) were detected. The concentration of doped copper in the glass was found to be 1.8 atomic percent using the survey spectra. The measured binding energies of B and O were found to be 192.3 eV and 532.2 eV, respectively [26]. The high-resolution spectra of Cu 2p analysis revealed distinct doublet peaks at energy levels of 934.8 eV and 954.8 eV. These peaks correspond to the Cu^{2+} 2p3/2 and Cu^{2+} 2p1/2 states, respectively [27]. Two prominent satellite peaks, distinct from the Cu peaks, were observed at 942.9 eV and 962.9 eV. The presence of these additional peaks in the satellite spectrum can be attributed to the $2p^{03}d^{9}$ electronic arrangement of Cu^{2+} in the CuO phase [28]. The difference in binding energy between spin orbits was 20 eV, which closely agreed with the previously reported values [27].

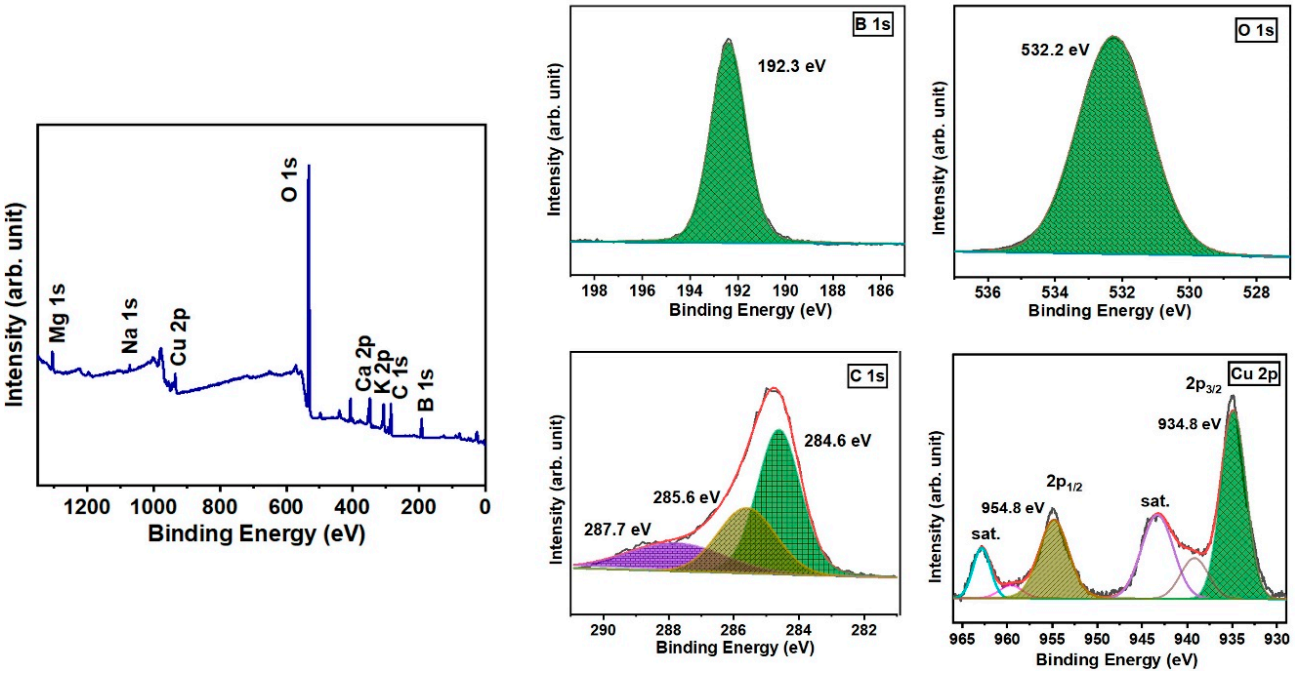

Figure 4. XPS survey spectra and high-resolution spectra of Cu-doped (0.25 M) borate bioactive glass.

3.3. Epifluorescence Microscopy Analysis

Figures 5 and 6 show epifluorescence microscopy images of *E. coli* and *S. aureus* in undoped and Cu-doped BBG. The image clearly shows that green fluorescence was observed in undoped BBG for both *E. coli* and *S. aureus* bacterial strains (white arrow), indicating minimal antibacterial activity. Furthermore, the addition of Cu to BBG lowered the survival rate of both bacterial strains over time. Figures 5 and 6b–d, exhibit primarily orange fluorescence, indicating bacterial death (*E. coli* and *S. aureus*). Cu influences the loss of membrane potential of the bacterial cell wall, resulting in the denatured state of proteins, amino acids, and DNA damage [29,30].

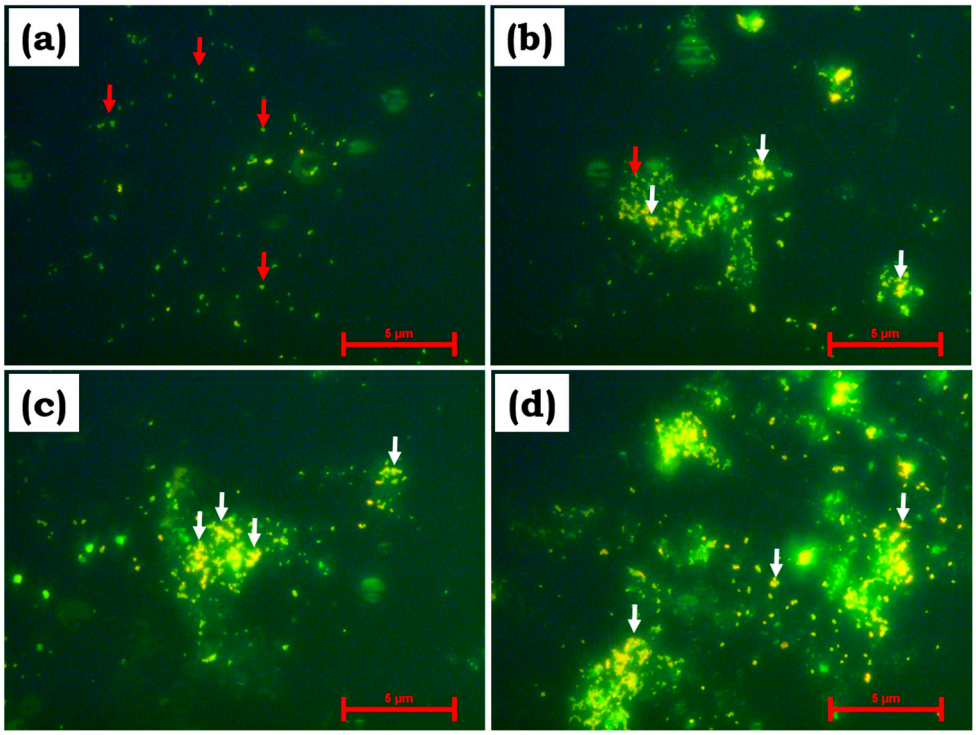

Figure 5. Epifluorescence microscopy images of (**a**) BBG, (**b**) 0.01 M Cu-doped BBG, (**c**) 0.05 M Cu-doped BBG, and (**d**) 0.25 M Cu-doped BBG against *E. coli*. Red arrow indicates live cells and white arrow indicates dead cells.

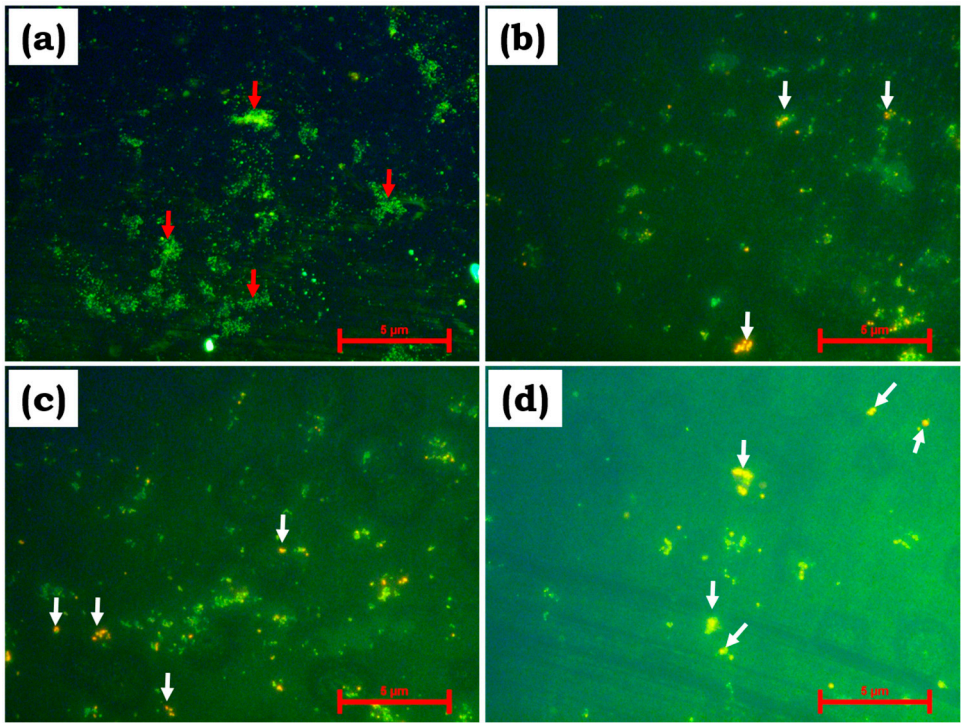

Figure 6. Epifluorescence microscopy images of (**a**) BBG, (**b**) 0.01 M Cu-doped BBG, (**c**) 0.05 M Cu-doped BBG, and (**d**) 0.25 M Cu-doped BBG against *S. aureus*. Red arrow indicates live cells and white arrow indicates dead cells.

3.4. Hydroxyl Radical Generation

Figure 7 demonstrates an increase in hydroxyl radical generation over time for all tested samples (undoped, 0.25 M Cu, and 0.05 M Cu). All samples of BBG have the property of generating OH radicals. While increasing the molarity of Cu, there is an increase in the OH concentration and ultimately a decrease in the growth of bacteria due to changes in cellular permeability. Notably, the rate of increase appears highest for the 0.25 M Cu-doped sample, followed by 0.05 M Cu and undoped samples. This suggests that a higher concentration of Cu (0.25 M) may accelerate hydroxyl radical formation. Mu et al. (2022) identified highly oxidative hydroxyl radicals (OH•) produced at normal temperatures, and their continuous synthesis can lead to the spontaneous oxidation of Cu ions [31]. This process might influence cellular membrane permeability and potentially contribute to further radical generation [11,31]. Bhattacharya et al. reported that BBG glasses inherently release OH radicals [13]. The observed antibacterial activity of Cu-doped BBG could be attributed to the combined effects of Cu-mediated hydroxyl radical generation and the inherent release of OH radicals from the BBG itself.

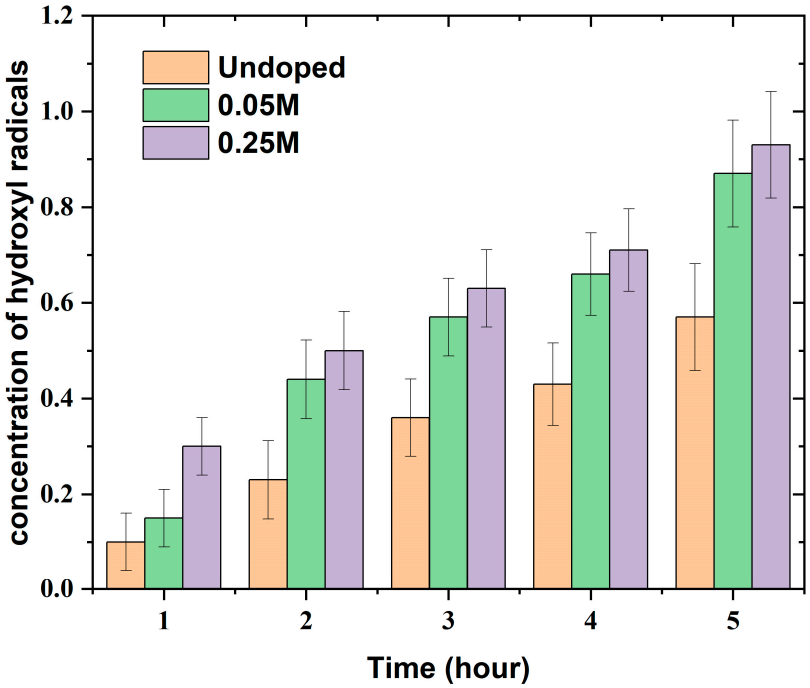

Figure 7. Free radical generation by Cu ion depicts oxidative damage to cellular events and organelles of the Gram-negative microbes.

3.5. Minimum Inhibitory Concentration (MIC)

The antibacterial activity of BBG, with a focus on its efficacy against both Gram-negative and Gram-positive bacteria, was assessed using a zone of inhibition assay. Notably, 0.25 M Cu-doped BBG showed substantial antibacterial action against *S. aureus* species. This finding suggests that Cu-doped BBG has potential relevance as an antibacterial agent, notably against the *S. aureus* strains listed in Table 2. More research may be required to clarify the mechanism of action and investigate the broader therapeutic implications.

Table 2. Minimum inhibitory concentrations of undoped and Cu-doped BBG.

BBG Powder	*E. coli* (Zone of Inhibition)	*S. aureus* (Zone of Inhibition)
BBG + 0.25 M Cu	16 mm	14 mm
BBG + 0.05 M Cu	10 mm	11 mm
BBG + 0.01 M Cu	8 mm	9 mm
Undoped BBG	4 mm	2 mm

3.6. Colony-Forming Unit (CFU)

The CFU for Cu doping reveals that the 0.25 M concentration may suppress the growth of both Gram-positive and Gram-negative microorganisms. This is because the CFU (colony-forming units) per microliter dropped at 0.25 M compared to the undoped control in both groups, as shown in Table 3. Interestingly, the 0.01 M concentration appears to stimulate Gram-negative microorganisms, resulting in a substantial increase in CFU compared to the control, but has the reverse effect on Gram-positive microbes. Further research is required to establish the particular mechanisms behind these observations [32,33].

Table 3. Colony-forming units per microliter (μL) of Gram-negative and Gram-positive microbes at different concentrations.

BBG Concentration (M)	*E. coli* (CFU/μL)	*S. aureus* (CFU/μL)
Undoped	2.79	2.67
0.25	1.11	1.07
0.05	2.01	1.33
0.01	269.0	2.77

3.7. Protein and Carbohydrate Discharge Assay

Anthrone and Bradford assays were used to quantify protein and carbohydrate discharge, respectively. These assays aimed to assess the ability of Cu-doped BBG to damage bacterial cells by disrupting their protein and carbohydrate structures. The data (Figures 8 and 9) reveal a trend of increasing protein and carbohydrate discharge from both *E. coli* and *S. aureus* as the copper concentration increases. Undoped BBG exhibited the least amount of discharge for both biomolecules, suggesting the dose-dependent effect of copper. This potentially indicates higher bacterial toxicity with increasing copper content. Bhattacharya et al. (2021) observed a similar correlation between bioactive glass concentration and the extent of molecule discharge. Free ions released from the bioactive glass are likely more effective at damaging cellular components and disrupting the cell wall compared to reactive ions [13].

Figure 8 depicts the protein discharge profile, whereas Figure 9 shows the carbohydrate discharge pattern. The observed changes in protein and carbohydrate discharge after BBG powder treatment suggest an alteration in bacterial proteomics and potentially a disruption of the peptidoglycan layer, which is the cell wall's upper layer composed of sugars and amino acids (Figure 10). Copper content appears to influence carbohydrate release, with a specific copper concentration (0.025 M) showing the highest discharge for *E. coli*. This pattern is consistent with observations for S. aureus. These findings suggest that copper may affect bacterial glucose leakage, potentially through altered membrane permeability or metabolic changes. This aligns with the observations of Bhattacharya et al. (2021) [13] who reported a higher impact of sugar discharge on Gram-positive bacteria compared to Gram-negative bacteria treated with Mg nanoparticles. Additionally, Toplitsch et al. (2021) found a correlation between antibacterial activity and the amount of Cu^{2+} generated by the samples [34].

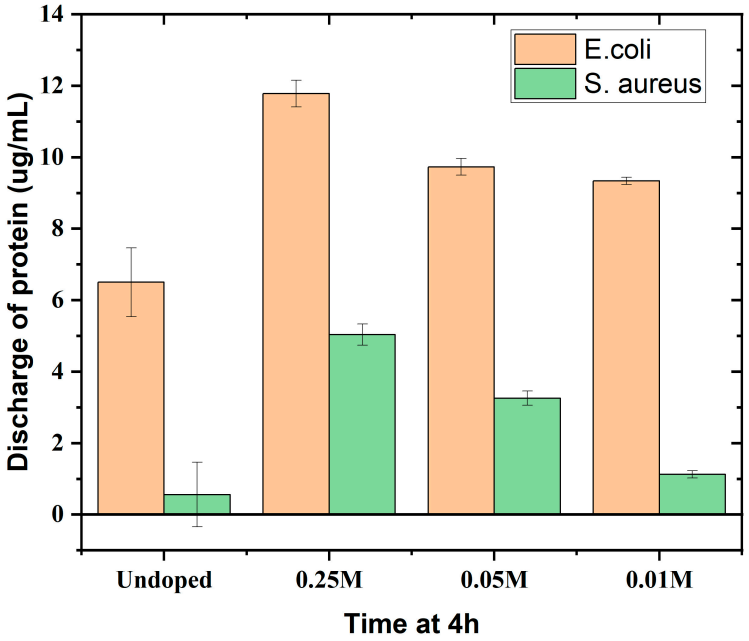

Figure 8. Protein discharge due to copper ion interaction with various cellular levels and its effect on antimicrobial activity.

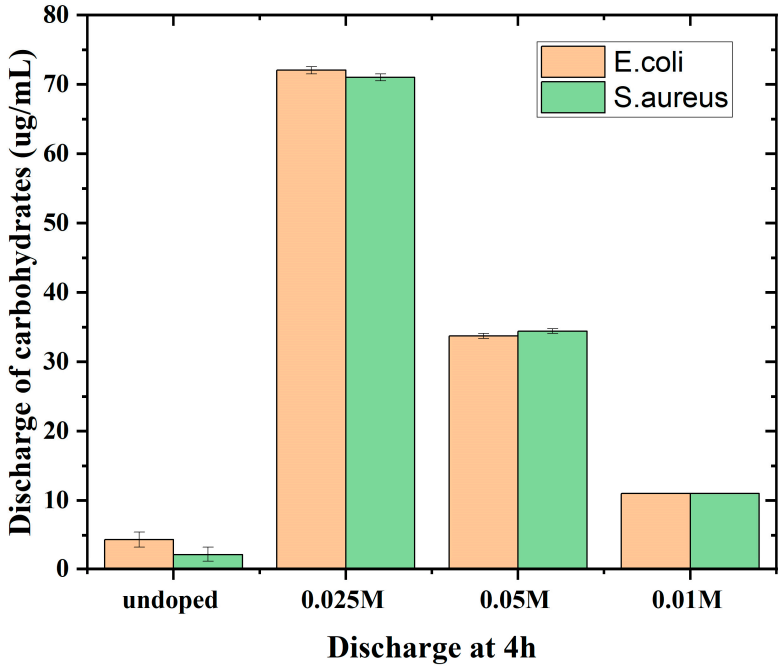

Figure 9. Carbohydrate discharge for different dopings of copper and their effect on antimicrobial activity.

Figure 10 shows a schematic diagram of the killing mechanism of bacteria on the copper surface. When the cell wall of the bacteria adheres to the Cu surface, the formation of oxidative stress followed by redox reactions triggers the reduction of Cu^{2+} and Cu^{+} ions in the presence of hydrogen peroxide (H_2O_2), which interacts with sulfur-containing and phosphorus compounds and subsequently damages deoxyribonucleic acid (DNA) [33]. Further, Cu^{2+} ions could enter bacterial cell walls through osmotic regulation and interact with intracellular amino acids and proteases, resulting in the denaturation of proteins [34]. Experimental data on protein, carbohydrate, and hydroxyl radical generation, as well as other antimicrobial assays, proved copper release to and metabolic disturbance in bacteria.

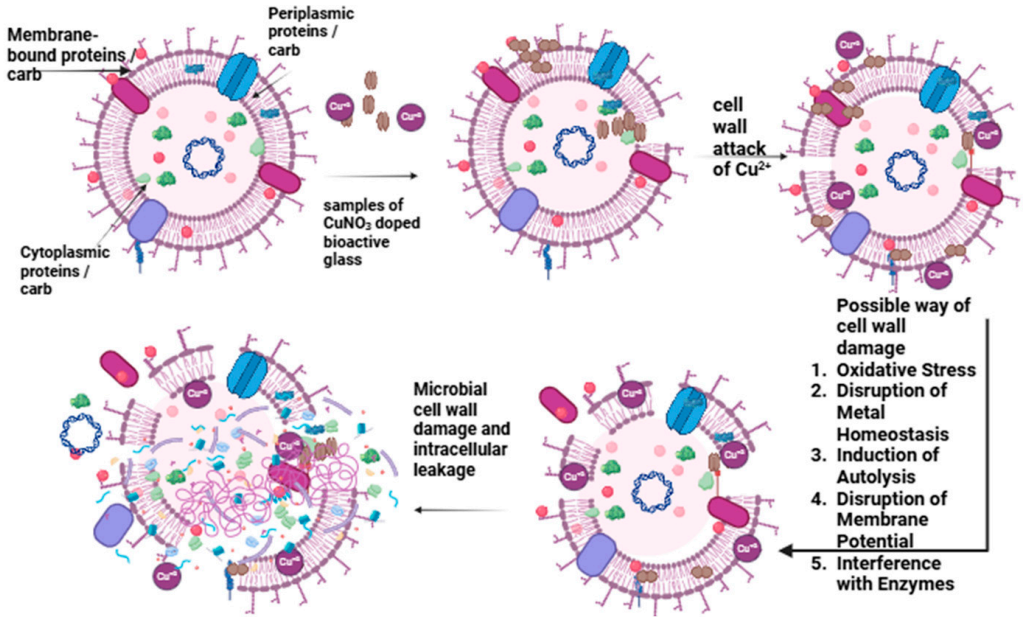

Figure 10. Schematic diagram of the mode of action of Cu-doped BBG powders.

4. Conclusions

This study successfully synthesized Cu-doped borate bioactive glass (BBG) using the sol–gel method. The presence of copper was confirmed using multiple techniques, and its concentration had a major impact on the BBG's properties. Increased copper concentrations resulted in smaller particle sizes and a shift from an amorphous to a more crystalline structure. An epifluorescence microscopy study demonstrated that Cu doping improved the BBG's antibacterial activity against both Gram-positive (*S. aureus*) and Gram-negative (*E. coli*) bacteria. Based on a study on hydroxyl radical generation, the presence of a certain concentration (0.25 M) may contribute to accelerated hydroxyl radical generation. The minimum inhibitory concentration (MIC) assay confirmed this finding, with 0.25 M Cu-doped BBG having the highest antibacterial activity. Interestingly, the CFU analysis revealed a concentration-dependent effect, with 0.25 M Cu suppressing microbial growth for both types of bacteria, whereas lower concentrations stimulated Gram-negative microorganisms. Protein and carbohydrate discharge experiments indicated that Cu-doped BBG destroys the bacterial cell wall and internal components, which contributes to its antibacterial activity. These findings highlight the potential of Cu-doped BBG as an antibacterial agent, notably against *S. aureus* strains. However, more research is needed to explain the mechanisms behind the reported results and investigate the material's broader therapeutic applications.

Author Contributions: Conceptualization, G.S.K. and B.S.; methodology, I.R., P.R., and B.S.; validation, K.K.A.M., G.S.K., and B.S.; formal analysis, I.R., P.R., and B.S.; investigation, B.S. and P.R.; data curation, P.R. and B.S.; writing—original draft preparation, I.R., P.R., and B.S.; writing—review and editing, K.K.A.M. and G.S.K.; supervision, G.S.K. and K.K.A.M. All authors have read and agreed to the published version of the manuscript.

Funding: This research was funded by the Biotechnology Industry Research Assistance Council (BIRAC) | Department of Biotechnology, under grant number "BIRAC SRISTI PMU 2021".

Data Availability Statement: Data are contained within the article.

Acknowledgments: The authors acknowledge the Chancellor, President and Vice Chancellor of the Sathyabama Institute of Science and Technology, Chennai, for providing the necessary facilities to carry out the research work.

Conflicts of Interest: The authors declare no conflicts of interest.

References

1. Pal, M.K.; Lavanya, M. Microbial Influenced Corrosion: Understanding Bioadhesion and Biofilm Formation. *J. Bio- Tribo-Corros.* **2022**, *8*, 76. [CrossRef]
2. Malard, F.; Dore, J.; Gaugler, B.; Mohty, M. Introduction to Host Microbiome Symbiosis in Health and Disease. *Mucosal Immunol.* **2020**, *14*, 547–554. [CrossRef]
3. Pugazhendhi, A.S.; Wei, F.; Hughes, M.; Coathup, M. Bacterial Adhesion, Virulence, and Biofilm Formation. In *Musculoskeletal Infection*; Springer: Cham, Switzerland, 2022; pp. 19–64. [CrossRef]
4. Bamford, N.C.; Macphee, C.E.; Stanley-Wall, N.R. Microbial Primer: An Introduction to Biofilms—What They Are, Why They Form and Their Impact on Built and Natural Environments. *Microbiology* **2023**, *169*, 001338. [CrossRef]
5. Krishnan, S. Biofilm Formation on Medical Devices and Infection: Preventive Approaches. In *Biofilm and Materials Science*; Springer: Cham, Switzerland, 2015; pp. 93–108. [CrossRef]
6. Troy, E.; Tilbury, M.A.; Power, A.M.; Wall, J.G. Nature-Based Biomaterials and Their Application in Biomedicine. *Polymers* **2021**, *13*, 3321. [CrossRef] [PubMed]
7. Kreve, S.; Reis, A.C.D. Bacterial Adhesion to Biomaterials: What Regulates This Attachment? A Review. *Jpn. Dent. Sci. Rev.* **2021**, *57*, 85–96. [CrossRef]
8. dos Santos, V.R.; Campos, T.M.B.; Anselmi, C.; Thim, G.P.; Bottino, M.C.; Borges, A.L.S.; Trichês, E. de S. Effect of Co, Cu, and Zn Ions on the Bioactivity and Antibacterial Properties of a Borate Bioactive Glass. *J. Non Cryst. Solids* **2023**, *622*, 122643. [CrossRef]
9. Harrison, J.J.; Tremaroli, V.; Stan, M.A.; Chan, C.S.; Vacchi-Suzzi, C.; Heyne, B.J.; Parsek, M.R.; Ceri, H.; Turner, R.J. Chromosomal Antioxidant Genes Have Metal Ion-Specific Roles as Determinants of Bacterial Metal Tolerance. *Environ. Microbiol.* **2009**, *11*, 2491–2509. [CrossRef] [PubMed]
10. Deliormanlı, A.M. Sol-Gel Synthesis of Borate-Based 13-93B3 Bioactive Glass Powders for Biomedical Applications. *Mater. Technol.* **2022**, *37*, 1808–1817. [CrossRef]
11. Babbs, C.F.; Gale Steiner, M. [11] Detection and Quantitation of Hydroxyl Radical Using Dimethyl Sulfoxide as Molecular Probe. *Methods Enzymol.* **1990**, *186*, 137–147. [CrossRef]
12. Steiner, M.G.; Babbs, C.F. Quantitation of the Hydroxyl Radical by Reaction with Dimethyl Sulfoxide. *Arch. Biochem. Biophys.* **1990**, *278*, 478–481. [CrossRef]
13. Bhattacharya, P.; Dey, A.; Neogi, S. An Insight into the Mechanism of Antibacterial Activity by Magnesium Oxide Nanoparticles. *J. Mater. Chem. B* **2021**, *9*, 5329–5339. [CrossRef] [PubMed]
14. Santos, L.H.M.L.M.; Insa, S.; Arxé, M.; Buttiglieri, G.; Rodríguez-Mozaz, S.; Barceló, D. Analysis of Microplastics in the Environment: Identification and Quantification of Trace Levels of Common Types of Plastic Polymers Using Pyrolysis-GC/MS. *MethodsX* **2023**, *10*, 102143. [CrossRef]
15. Lepry, W.C.; Smith, S.; Nazhat, S.N. Effect of Sodium on Bioactive Sol-Gel-Derived Borate Glasses. *J. Non Cryst. Solids* **2018**, *500*, 141–148. [CrossRef]
16. Bento, R.; Gaddam, A.; Ferreira, J.M.F. Sol–Gel Synthesis and Characterization of a Quaternary Bioglass for Bone Regeneration and Tissue Engineering. *Materials* **2021**, *14*, 4515. [CrossRef]
17. Sreedhar, M.; Reddy, I.N.; Bera, P.; Ramachandran, D.; Gobi Saravanan, K.; Rabel, A.M.; Anandan, C.; Kuppusami, P.; Brijitta, J. Cu/TiO_2 Thin Films Prepared by Reactive RF Magnetron Sputtering. *Appl. Phys. A Mater. Sci. Process* **2015**, *120*, 765–773. [CrossRef]
18. Konijnendijk, W.L.; Stevels, J.M. Structure of Borate and Borosilicate Glasses by Raman Spectroscopy. In *Borate Glasses*; Springer: Boston, MA, USA, 1978; pp. 259–279. [CrossRef]
19. Padmaja, G.; Kistaiah, P. Infrared and Raman Spectroscopic Studies on Alkali Borate Glasses: Evidence of Mixed Alkali Effect. *J. Phys. Chem. A* **2009**, *113*, 2397–2404. [CrossRef] [PubMed]
20. de Souza, J.R.; Kukulka, E.C.; Araújo, J.C.R.; Campos, T.M.B.; do Prado, R.F.; de Vasconcellos, L.M.R.; Thin, G.P.; Borges, A.L.S. Electrospun Polylactic Acid Scaffolds with Strontium- and Cobalt-Doped Bioglass for Potential Use in Bone Tissue Engineering Applications. *J. Biomed. Mater. Res. B Appl. Biomater.* **2023**, *111*, 151–160. [CrossRef] [PubMed]
21. Liu, A.; Shi, Z.; Reddy, R.G. Mechanism Study of Cu-Zn Alloys Electrodeposition in Deep Eutectic Solvents. *Ionics* **2020**, *26*, 3161–3172. [CrossRef]
22. Siddiqui, H.; Parra, M.R.; Qureshi, M.S.; Malik, M.M.; Haque, F.Z. Studies of Structural, Optical, and Electrical Properties Associated with Defects in Sodium-Doped Copper Oxide (CuO/Na) Nanostructures. *J. Mater. Sci.* **2018**, *53*, 8826–8843. [CrossRef]
23. ElBaz, N.; El-Damrawi, G.; Abdelghany, A.M.; ElBaz, N.; El-Damrawi, G.; Abdelghany, A.M. Structural Role of CeO_2 in the Modified Borate Glass-Ceramics. *New J. Glass Ceram.* **2021**, *11*, 34–43. [CrossRef]
24. Iqbal, M.; Ali, A.; Ahmad, K.S.; Rana, F.M.; Khan, J.; Khan, K.; Thebo, K.H. Synthesis and Characterization of Transition Metals Doped CuO Nanostructure and Their Application in Hybrid Bulk Heterojunction Solar Cells. *SN Appl. Sci.* **2019**, *1*, 647. [CrossRef]
25. Lallukka, M.; Miola, M.; Najmi, Z.; Cochis, A.; Spriano, S.; Rimondini, L.; Verné, E. Cu-Doped Bioactive Glass with Enhanced In Vitro Bioactivity and Antibacterial Properties. *Ceram. Int.* **2024**, *50*, 5091–5103. [CrossRef]
26. Senna, M.; Noda, H.; Xin, Y.; Hasegawa, H.; Takai, C.; Shirai, T.; Fuji, M. Solid-State Reduction of Silica Nanoparticles via Oxygen Abstraction from SiO_4 Units by Polyolefins under Mechanical Stressing. *RSC Adv.* **2018**, *8*, 36338. [CrossRef] [PubMed]
27. Nandanwar, S.; Borkar, S.; Cho, J.H.; Kim, H.J. Microwave-assisted Synthesis and Characterization of Solar-Light-active Copper–Vanadium Oxide: Evaluation of Antialgal and Dye Degradation Activity. *Catalysts* **2021**, *11*, 36. [CrossRef]

28. Svintsitskiy, D.A.; Yu Kardash, T.; Boronin, A.I. Surface Dynamics of Mixed Silver-Copper Oxide $AgCuO_2$ during X-ray Photoelectron Spectroscopy Study. *Appl. Surf. Sci.* **2019**, *463*, 300–309. [CrossRef]
29. Kumar, D.D.; Kaliaraj, G.S. Multifunctional Zirconium Nitride/Copper Multilayer Coatings on Medical Grade 316L SS and Titanium Substrates for Biomedical Applications. *J. Mech. Behav. Biomed. Mater.* **2018**, *77*, 106–115. [CrossRef] [PubMed]
30. Chatterjee, A.K.; Chakraborty, R.; Basu, T. Mechanism of Antibacterial Activity of Copper Nanoparticles. *Nanotechnology* **2014**, *25*, 135101. [CrossRef] [PubMed]
31. Mu, S.; Lu, H.; Wu, Q.; Li, L.; Zhao, R.; Long, C.; Cui, C. Hydroxyl Radicals Dominate Reoxidation of Oxide-Derived Cu in Electrochemical CO_2 Reduction. *Nat. Commun.* **2022**, *13*, 3694. [CrossRef] [PubMed]
32. Rundén-Pran, E.; Mariussen, E.; El Yamani, N.; Elje, E.; Longhin, E.M.; Dusinska, M. The Colony Forming Efficiency Assay for Toxicity Testing of Nanomaterials—Modifications for Higher-Throughput. *Front. Toxicol.* **2022**, *4*, 983316. [CrossRef] [PubMed]
33. Pan, H.; Zhang, Y.; He, G.X.; Katagori, N.; Chen, H. A Comparison of Conventional Methods for the Quantification of Bacterial Cells after Exposure to Metal Oxide Nanoparticles. *BMC Microbiol.* **2014**, *14*, 222. [CrossRef]
34. Toplitsch, D.; Lackner, J.M.; Schwan, A.M.; Hinterer, A.; Stögmüller, P.; Horn, K.; Fritzlar, N.; Pfuch, A.; Kittinger, C. Antimicrobial Activity of a Novel $Cu(NO_3)_2$-Containing Sol–Gel Surface under Different Testing Conditions. *Materials* **2021**, *14*, 6488. [CrossRef] [PubMed]